2020 IEEE International Conference on Robotics and Automation (ICRA)
31 May - 31 August, 2020. Paris, France

Fast, Versatile, and Open-loop Stable Running Behaviors with Proprioceptive-only Sensing using Model-based Optimization

Wei Gao, Charles Young, John Nicholson, Christian Hubicki and Jonathan Clark*

***Abstract*— As we build our legged robots smaller and cheaper, stable and agile control without expensive inertial sensors becomes increasingly important. We seek to enable versatile dynamic behaviors on robots with limited modes of state feedback, specifically proprioceptive-only sensing. This work uses model-based trajectory optimization methods to design open-loop stable motion primitives. We specifically design running gaits for a single-legged planar robot, and can generate motion primitives in under 3 seconds, approaching online-capable speeds. A direct-collocation-formulated optimization generated axial force profiles for the direct-drive robot to achieve desired running speed and apex height. When implemented in hardware, these trajectories produced open-loop stable running. Further, the measured running achieved the desired speed within 10% of the speed specified for the optimization in spite of having no control loop actively measuring or controlling running speed. Additionally, we examine the shape of the optimized force profile and observe features that may be applicable to open-loop stable running in general.**

I. INTRODUCTION

The fact that legged animals in the natural world can traverse diverse terrains with great agility has inspired researchers to develop a variety of legged robots. To emulate dynamic and adaptive legged locomotion observed on animals, these robots need not only robust leg controllers for one environment, but also advanced techniques that can optimize the controllers for various environment on-the-fly.

Leg controllers are often bio-inspired, to duplicate the major functionality of biological systems through straightforward mechatronic design and clever control laws. They are then simulated upon system models and verified through experiments. As a reduced-order model, the Spring-Loaded Inverted Pendulum (SLIP) model has been shown to capture the whole-body dynamics of a wide range of animals' locomotion [1], [2] and was key to the first dynamic running robots pioneered by Raibert et al. [3]. These robots used an impulse-based scheme (instantaneous increase in spring stiffness at maximum compression) to move quickly, while other early running robots such as RHex and iSprawl relied upon time-based, open-loop schemes and the passive dynamics of their legs [4], [5]. Subsequent studies have suggested other time-based control policies including prescribing a sinusoidal profile for the rest length of leg spring during the stance phase (AER) [6], or mixing rest length extension with a softening spring stiffness [7]. Variants of these open-loop approaches to control continue to be used for small, computationally limited robots such as DASH, HAMR, and others [8], [9], [10].

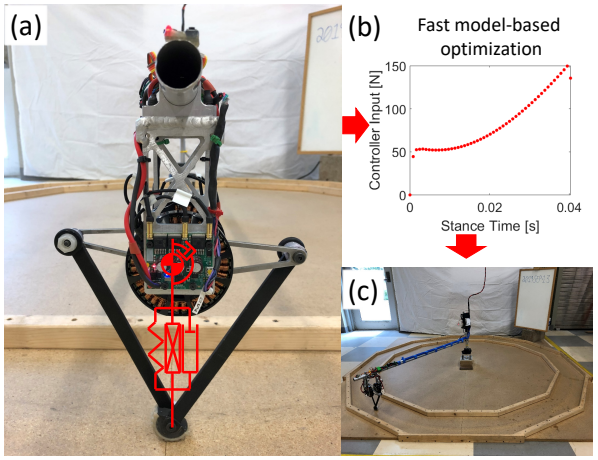

Fig. 1. Overview. (a) A single-legged hopper with reduced-order model superimposed. (b) Fast model-based optimization generates controller force profile in 3 s. (c) Open-loop stable running achieves average forward velocity of 3.8 m/s.

No matter it is stiffness modulation or rest length modulation or the two combined, eventually the controller is modulating the leg force based on time during the stance phase. As long as an optimized time-based force profile can be generated, it is only a matter of translating the force profile into stiffness profile and/or rest length profile. Although leg force optimization in simulation has been performed before [11], it was for specific applications and the results were not as general as shown in this paper. More importantly, the optimization techniques presented were not for real-time implementation, such that adaptive legged locomotion could not be achieved. Experimental optimizations were previously implemented on running platforms, which have successfully developed high-speed gaits (2.7 m/s for RHex [12], and 3.0 m/s for Minitaur [13]), but these experiments have been very costly, taking tens of hours each.

Robotics in general has made use of increasingly powerful online optimization techniques to achieve versatile locomotion. The DARPA robotics challenge was a showcase of real-time planners for robots with full actuation [14]. More recently, model-predictive control (MPC) methods have been used for highly dynamic quadruped maneuvers, providing over 100 Hz computation for systems with linear dynamics [15]. Differential Dynamic Programming (DDP) also provides fast methods for trajectory generation in the presence of underactuation [16]. For nonlinear robot models

*Department of Mechanical Engineering, FAMU-FSU College of Engineering, Florida State University, Tallahassee, Florida 32310, USA clarkj@eng.famu.fsu.edu

with hard control constraints (like dynamic gait optimization in this paper), researchers have used model-based nonlinear programming (NLP) solvers like IPOPT [17] to achieve 1-second optimization for walking maneuvers [18]. Fast and stable running gaits have also been realized on bipedal running robots using these techniques based on hybrid zero dynamics (HZD) [19], [20]. This work applies NLP methods to achieve fast running optimization using the simple SLIP-based model.

The paper takes time-based spring modulation as a potentially robust leg controller, and utilizes advanced optimization techniques that can generate force profiles for desired gaits within seconds. The physical platform, see Figure 1, actuated by these optimal force profiles is shown to achieve the expected gaits successfully. The remainder of the paper first demonstrates the physical platform that is used to realize spring modulation in Section II. Based upon the physical platform, dynamic models of the system are developed in Section III. Time-based force modulation as the controller is then optimized in Section IV. Section V sees the experimental results as verification of the obtained optimal force profiles. Conclusions are drawn in Section VI.

II. PHYSICAL PLATFORM

SLIP-like runners have shown great success in robust legged locomotion. The SLIP-like runner used for spring modulation in this paper is a single-legged hopper as shown in Figure 1(a). The leg comes from the Minitaur quadrupedal platform [21]. It has a five-bar mechanism driven by two co-axial Tiger U8 brushless DC motors at the hip, thus a virtual spring can be imagined to connect the hip and the foot, as well as a damper and an actuator in parallel. Through modulating the control effort of hip motors, force modulation by the actuator to the virtual leg spring can be achieved.

Among the five links in the leg, one is the u-shape bracket that connects stators of the two motors, two are the proximal links of length $0.1\,\mathrm{m}$ that are attached to rotors of the two motors, and two are the distal links of length $0.2\,\mathrm{m}$ that are connected to the proximal ones at the knees and also interconnected at the ankle. The revolute joints at the two knees and the ankle are all passive. Leg links were previously fabricated from aluminum using waterjet machining. Currently, only the proximal links are made from aluminum, while the distal links and foot were revised to be 3D printed for a $48\,\%$ reduction of the distal mass. This improvement was achieved using a Markforged Mark Two printer with Onyx filament and continuous carbon fiber reinforcement. The foot extension at the ankle is made of a 3D printed structure with a tread layer to produce high friction and avoid slippage. The foot's printed substrate is comprised entirely of Markforged Onyx material, and the elastomeric tread is overmolded using Smooth-On VytaFlex 60 urethane.

Hall Effect based absolute encoders located on the hip motors provide the motor positions as feedback signals to facilitate closed-loop control of the leg position. An aluminum tube of length $1.15\,\mathrm{m}$ holds the leg at the u-shape bracket and allows it to do spherical movement around the base freely, as shown in Figure 1(c). With large radius and small polar angle, the leg is assumed to be moving in the sagittal plane along the wooden track. Two Accu-Coder model 15s encoders are located at the base of the boom, which operate in the quadrature phase and measure the azimuth and polar angles of the tube. All the data are recorded via a Teensy 3.6 microcontroller at $500\,\mathrm{Hz}$, while the control frequency for the leg is set at $1000\,\mathrm{Hz}$. The major physical parameters of the robot are shown in Table I. Note that the nominal leg rest length l_o is determined when the proximal links are placed in horizontal configuration, and the nominal leg stiffness k_o is set to the value scaled from human data (mass = $80\,\mathrm{kg}$, nominal leg rest length = $1\,\mathrm{m}$, nominal leg stiffness = $19\,600\,\mathrm{N/m}$) [7].

TABLE I
MAJOR SYSTEM PARAMETER VALUES.

Name	Symbol	Value
Gravitational Acceleration	g	$9.8\,\mathrm{m/s^2}$
Mass at the Hip	m	$1.2\,\mathrm{kg}$
Nominal Leg Rest Length	l_o	$0.1732\,\mathrm{m}$
Nominal Leg Stiffness	k_o	$1697\,\mathrm{N/m}$
Leg Linear Damping	b_l	$12.6371\,\mathrm{N\,s/m}$
Hip Torsional Damping	b_t	$0.0812\,\mathrm{N\,m\,s/rad}$
Proximal Link Length	l_1	$0.1\,\mathrm{m}$
Distal Link Length	l_2	$0.2\,\mathrm{m}$

III. SIMULATION MODEL

A. The Force-Driven and Damped SLIP Model

To match the physical platform, a force-driven and damped SLIP (FD-SLIP) model is developed, as shown in Figure 2. Compared to the SLIP model, the FD-SLIP model has a linear damper and an actuator in parallel to the leg spring, and an additional torsional damper around the hip.

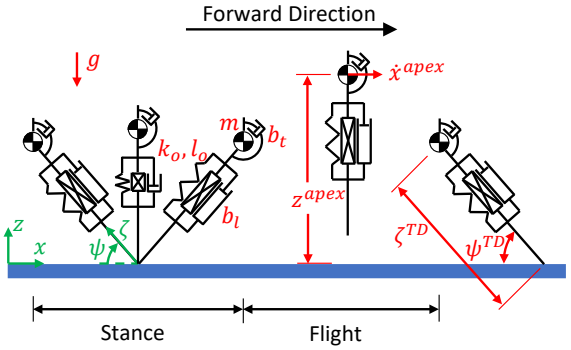

Fig. 2. A sketch of the FD-SLIP model.

A single step of the FD-SLIP model consists of a stance phase and a flight phase. The transition event from stance phase to flight phase is defined as liftoff, and from flight phase to stance phase is defined as touchdown. During the stance phase, because the foot is pinned down to the ground,

the system can be conveniently described in polar coordinates (ζ, ψ), with ζ being leg length from the foot to the hip and ψ being leg angle measured clockwise from the ground to the leg (the smaller angle of the two). The equations of motion for the stance phase can be derived as

$$\begin{cases} \ddot{\zeta} = \zeta\dot{\psi}^2 - g\sin\psi - \dfrac{k_o}{m}(\zeta - l_o) - \dfrac{b_l}{m}\dot{\zeta} + \dfrac{u}{m}, \\ \ddot{\psi} = -\dfrac{2\dot{\zeta}\dot{\psi}}{\zeta} - \dfrac{g\cos\psi}{\zeta} - \dfrac{b_t}{m\zeta^2}\dot{\psi}, \end{cases} \tag{1}$$

where u is the force input from the actuator. The effect of different flight phase controllers is beyond the scope of this paper, so a minimal functional controller is adopted, resetting the leg to its desired touchdown angle ψ^{TD} after liftoff [22]. As a result, the system is only affected by gravity during the flight phase where its motion is conveniently described in Cartesian coordinates (x, z), with x and z being the horizontal and vertical positions of the body, respectively. The equations of motion can be easily derived as

$$\begin{cases} \ddot{x} = 0, \\ \ddot{z} = -g. \end{cases} \tag{2}$$

Note that the equations of motion for the stance phase cannot be analytically solved, while those for the flight phase can, which simplifies the optimization setup that is discussed in Section IV.

B. The Spring Modulation Controller

The term u in Equation (1) is supposed to follow the force profile applied by the controller. However, the spring modulation controller on the physical platform is implemented in the motor space instead of the virtual leg space. Therefore, a mapping between the two spaces is necessary. A sketch visually showing the relationship between the two spaces can be found in Figure 3. The angular positions of two hip motors are represented by ψ_1 and ψ_2, respectively, measured from the negative z direction to the corresponding links.

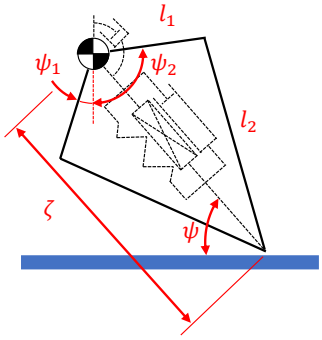

Fig. 3. A sketch illustrating the mapping between the physical leg (solid lines) and the virtual leg (dash lines).

Due to symmetry of the leg, the length ζ and angle ψ of the virtual leg can be written as

$$\begin{cases} \zeta = l_1\cos\dfrac{\psi_1 + \psi_2}{2} + \sqrt{l_2^2 - l_1^2\sin^2\dfrac{\psi_1 + \psi_2}{2}}, \\ \psi = \dfrac{\pi}{2} - \dfrac{\psi_1 - \psi_2}{2}. \end{cases} \tag{3}$$

From Equation (3), the Jacobian matrix J relating the motors' angular velocities to the virtual leg's linear and angular velocities in

$$\begin{pmatrix} \dot{\zeta} \\ \dot{\psi} \end{pmatrix} = J \begin{pmatrix} \dot{\psi}_1 \\ \dot{\psi}_2 \end{pmatrix} \tag{4}$$

can be derived as

$$J = \begin{bmatrix} J_{11} & J_{12} \\ J_{21} & J_{22} \end{bmatrix} = \begin{bmatrix} \dfrac{\partial\zeta}{\partial\psi_1} & \dfrac{\partial\zeta}{\partial\psi_2} \\ \dfrac{\partial\psi}{\partial\psi_1} & \dfrac{\partial\psi}{\partial\psi_2} \end{bmatrix}, \tag{5}$$

where

$$\begin{cases} J_{11} = J_{12} = \\ \qquad -\dfrac{l_1}{2}\sin\dfrac{\psi_1 + \psi_2}{2} - \dfrac{l_1^2\sin\dfrac{\psi_1 + \psi_2}{2}\cos\dfrac{\psi_1 + \psi_2}{2}}{2\sqrt{l_2^2 - l_1^2\sin^2\dfrac{\psi_1 + \psi_2}{2}}}, \\ J_{21} = -\dfrac{1}{2}, \\ J_{22} = \dfrac{1}{2}. \end{cases} \tag{6}$$

The Jacobian matrix J can also be used to relate leg forces to motor torques as in

$$\begin{pmatrix} F_\zeta \\ \tau_\psi \end{pmatrix} = J^{-T} \begin{pmatrix} \tau_1 \\ \tau_2 \end{pmatrix}, \tag{7}$$

where F_ζ is the force along the leg, τ_ψ is the torque around the hip, and τ_1 and τ_2 are the corresponding torques applied by the two hip motors. To relate back to Equation (1), the force F_ζ in Equation (7) can be written as

$$F_\zeta = -k_o(\zeta - l_o) + u, \tag{8}$$

while the torque τ_ψ is always set to zero to allow free rotation during the stance phase. Consequently, by commanding motor torques τ_1 and τ_2 in Equation (7), the desired leg force F_ζ, or the desired force input u, can be achieved.

The force modulation profile for u, as mentioned in Section I, can be further interpreted as either stiffness modulation or rest length modulation based on Equation (8):

$$F_\zeta = -(k_o - \frac{u}{\zeta - l_o})(\zeta - l_o) \tag{9}$$

or

$$F_\zeta = -k_o[\zeta - (l_o + \frac{u}{k_o})]. \tag{10}$$

Note that when the force modulation is interpreted as stiffness modulation, the effective stiffness is based on not only time, but also state ζ, which makes the case more complicated than being interpreted as rest length modulation.

IV. CONTROL OPTIMIZATION

Obtaining the optimal time-based force profiles for the stance phase involves solving a trajectory optimization problem. To achieve stable running gaits, the optimization process should at least fulfill two tasks: identify periodic gaits, or limit cycles, and evaluate the stability of those limit cycles. Conventional approach for searching limit cycles

would assign one set of possible controller parameter values each time, integrate the system dynamics via time-marching numerical methods, and adjust the system initial states according to gradient based methods until the requirements for limit cycles are met. This approach is generally called the direct single shooting method. It can provide rich information about the controller parameter space when the dimension of that space is relatively small (less than five), thus insights can be extracted. However, it becomes intractable quickly when the dimension grows bigger, which is exactly the case in this paper. To describe an arbitrary and smooth time-based force profile, given the typical stance time for the single-legged hopper is on the order of tens of milliseconds and the controller updates every millisecond, the required number of way points on the profile can easily go above ten, which means more than ten controller parameter values need to be optimized. Therefore, a better suited trajectory optimization technique, called direct collocation, is adopted to solve the problem [23], using algebraic constraints to solve system dynamics instead of the aforementioned time-marching method. We use IPOPT as the NLP solver. As a result, the optimization can be accomplished within seconds rather than several hours or even days for conventional controller parameter sweeps. Although detailed information about the controller parameter space is lost in this manner, the fast optimization speed makes it promising for real-time application on a physical platform.

Because the leg length at touchdown, ζ^{TD}, is always set to the nominal leg rest length, l_o, a gait of the system can be characterized by three variables: touchdown leg angle ψ^{TD}, apex height z^{apex}, and apex horizontal velocity $\dot{x}^{apex}$. Given an apex height and horizontal velocity, the system can be analytically solved for the flight phase according to Equation (2), yielding boundary conditions for the stance phase. Therefore, the optimization only needs to deal with the stance phase. The optimization problem can then be mathematically stated as

$$\begin{aligned}
\text{argmin} \quad & \sum_{t=t^{TD}}^{t^{LO}} [u(t)]^2, \\
\text{s.t.} \quad & \dot{\boldsymbol{s}}(t) = F[t, \boldsymbol{s}(t), u(t)], \\
& G[t, \boldsymbol{s}(t), u(t)] \geq 0, \\
& H[t^{TD}, \boldsymbol{s}(t^{TD}), u(t^{TD}), t^{LO}, \boldsymbol{s}(t^{LO}), u(t^{LO})] \geq 0,
\end{aligned} \tag{11}$$

where t is time, $\boldsymbol{s}$ is the system state vector ($\boldsymbol{s} = [\zeta, \dot{\zeta}, \psi, \dot{\psi}]^T$), superscript TD stands for the moment of touchdown, superscript LO stands for the moment of liftoff, F represents the dynamic constraint that is the state space form of Equation (1), G represents the trajectory constraint that includes ground reaction force and motor model, and H represents boundary constraint that contains touchdown and liftoff conditions. Note that the cost function adopted in Equation (11) is the sum of squared force input required to achieve the limit cycle, which is related to efficiency of the gait. Other reasonable cost functions could also be used, such as stance time [11]. Explicitly, the trajectory constraint G can be written as

$$\begin{cases}
[-k_o(\zeta - l_o) - b_l\dot{\zeta} + u]\sin\psi - b_t\dot{\psi}\cos\psi/\zeta \geq 0, \\
|\tau_{1,2}| \leq \tau_{stall}(1 - \dfrac{|\dot{\psi}_{1,2}|}{\omega_{NL}}),
\end{cases} \tag{12}$$

where the first expression requires the ground reaction force to be non-negative during the stance phase and the second expression reveals a linear torque-speed curve in the motor model. The expressions for $\dot{\psi}_{1,2}$ and $\tau_{1,2}$ can be derived from Equations (4) and (7), and the subscript $1, 2$ just means the two motors share the same model. The stall torque and no-load speed are rated to be: $\tau_{stall} = 7.69\,\mathrm{N\,m}$ and $\omega_{NL} = 158\,\mathrm{rad/s}$. On the other hand, the boundary constraint H can be demonstrated separately as touchdown conditions

$$\begin{cases}
\zeta(t^{TD}) = l_o, \\
\dot{\zeta}(t^{TD}) = \\
-\dot{x}^{apex}\cos\psi^{TD} - \sqrt{2g(z^{apex} - l_o\sin\psi^{TD})}\sin\psi^{TD}, \\
\psi(t^{TD}) = \psi^{TD}, \\
\dot{\psi}(t^{TD}) = \\
[\dot{x}^{apex}\sin\psi^{TD} - \sqrt{2g(z^{apex} - l_o\sin\psi^{TD})}\cos\psi^{TD}]/l_o, \\
u(t^{TD}) = 0,
\end{cases} \tag{13}$$

and liftoff conditions

$$\begin{cases}
\zeta(t^{LO})\dot{\psi}(t^{LO})\sin\psi(t^{LO}) - \dot{\zeta}(t^{LO})\cos\psi(t^{LO}) = \dot{x}^{apex}, \\
[\zeta(t^{LO})\dot{\psi}(t^{LO})\cos\psi(t^{LO}) + \dot{\zeta}(t^{LO})\sin\psi(t^{LO})]^2/(2g) \\
\qquad\qquad + \zeta(t^{LO})\sin\psi(t^{LO}) = z^{apex}, \\
\dot{\zeta}(t^{LO}) \geq 0, \\
\dot{\zeta}(t^{LO})\sin\psi(t^{LO}) + \zeta(t^{LO})\dot{\psi}(t^{LO})\cos\psi(t^{LO}) \geq 0, \\
\{-k_o[\zeta(t^{LO}) - l_o] - b_l\dot{\zeta}(t^{LO}) + u(t^{LO})\}\sin\psi(t^{LO}) \\
\qquad\qquad - b_t\dot{\psi}(t^{LO})\cos\psi(t^{LO})/\zeta(t^{LO}) = 0.
\end{cases} \tag{14}$$

The optimization was implemented in MATLAB 2018b using the COALESCE toolbox [24] and executed for a range of $[\dot{x}^{apex}, z^{apex}, \psi^{TD}]$ to seek the corresponding optimal force profile u. By satisfying all the constraints, the yielded gaits are automatically limit cycles. The stability of each limit cycle is then evaluated by the maximum Floquet multiplier [25]. The ranges swept for $[\dot{x}^{apex}, z^{apex}, \psi^{TD}]$ are, in turn, from $1.5\,\mathrm{m/s}$ to $4\,\mathrm{m/s}$ with an increment of $0.5\,\mathrm{m/s}$, from $0.18\,\mathrm{m}$ to $0.27\,\mathrm{m}$ with an increment of $0.01\,\mathrm{m}$, and from 60° to 89° with an increment of 1°. A stability distribution map is thus obtained as shown in Figure 4. The horizontal axis represents the apex horizontal velocity and the vertical axis represents the apex height. While multiple gaits can be found at each combination of apex height and velocity due to different touchdown angles, the color indicates performance of the most stable gait. Note that the distribution map only shows the stability of the optimal gait obtained from trajectory optimization. For example, it indicates that the gait with apex horizontal velocity of $4\,\mathrm{m/s}$ and apex height of $0.18\,\mathrm{m}$ can be optimized to be the most stable. However, it

does not imply that the gait tends to be more stable with lower apex height and faster apex horizontal velocity. This is the shortcoming of this two-layer style optimization. In the future, it is desired to merge the stability evaluation into the optimization process. This may require clever design of the cost function and is beyond the scope of this paper.

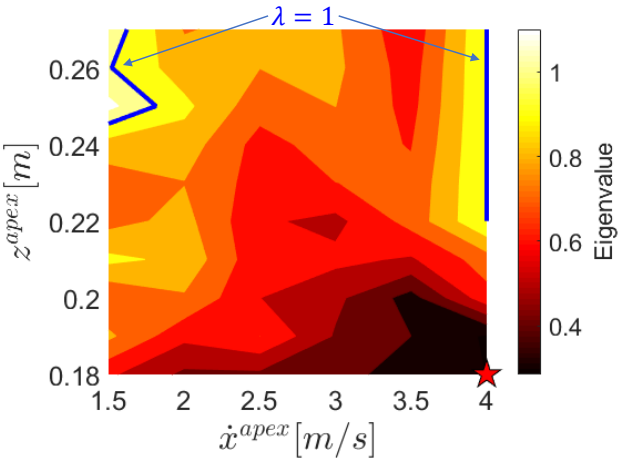

Fig. 4. Stability distribution of the gaits driven by optimal force profiles. The eigenvalue λ is defined as the maximum Floquet multiplier.

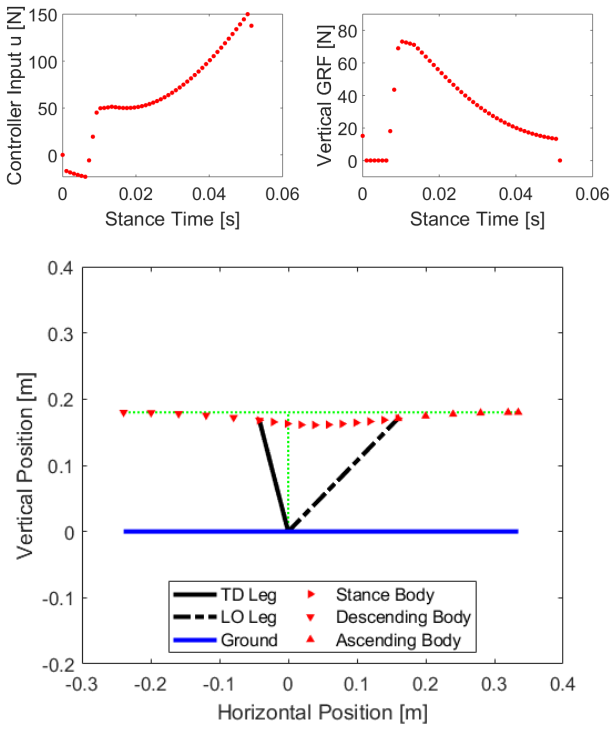

Fig. 5. Details of the red star gait in Figure 4, with the top left plot being the optimal force profile, the top right plot being the vertical ground reaction force (GRF) profile, and the bottom plot being the Center of Mass trajectory from one apex point to the next.

Based upon the stability distribution map, the generated optimal force profiles can better stabilize the gaits with high apex horizontal velocities and low apex heights. To explore the reasons behind, a typical gait marked by the star in Figure 4 is selected and the corresponding optimal force profile, vertical ground reaction force profile and Center of Mass (CoM) trajectory are plotted in Figure 5. It appears that there are generally three stages for the optimal force profile. The first stage involves a portion of negative force input once the leg starts breaking at the beginning of the stance phase. The vertical ground reaction force at this stage is mitigated to zero. The second stage is a transition from the first stage to the third where an abrupt change in the force profile happens, from negative to positive values. This happens when the leg vaults over the upright direction, switching from breaking mode to thrusting mode. Once enters the third stage, the force input starts ramping up to accelerate the system, first slowly and then quickly, until liftoff happens. This optimal force profile shares the flavors of the fixed thrust (FT) controller [6] where there is an abrupt force increase around maximum leg compression and the AER controller where the force profile follows a sinusoidal trajectory when ramping up. It can potentially inspire new leg controllers in future work where online optimization is not feasible, such as gram scale microrobots [26], [27].

V. EXPERIMENTAL VERIFICATION

To implement the optimal force profile on the physical platform, several issues were addressed. First, the optimal force profile is generated separately from the main controller board's Arduino 1.6.1 code and must be uploaded prior to each experimental run. The force profile data array is transmitted via USB-TTL serial communication from MATLAB 2018b to the main controller board where it is stored. The controller code later calls the stored array to apply the correct force input when stance phase is triggered. Second, real-time datalogging is needed to simultaneously collect data from the physical platform and main controller board that is communicated via serial communication. A Teensy 3.6 microcontroller stores the data to a micro SD card to allow for post-processing. This dataset includes: the platform's two angular encoders located at its base and boom arm, current sensing of the motor controllers' inputs, and the virtual-leg calculations that result from the main controller board's access to motor encoders located at the hip axis.

Additionally, the physical platform has a software-based, touchdown delay mechanism to reduce erroneous stance phase triggering and enable robust running performance. The touchdown delay mechanism consists of two stages, the first requires a positive leg compression such that the estimated leg force passes a threshold to initiate the touchdown signal, and the second requires the touchdown signal to last for seven consecutive milliseconds to trigger the stance phase. The same procedure is used to trigger flight phase, but it has a less significant impact on the force profile optimization. The empirical force threshold used for touchdown is $10\,\mathrm{N}$. Accordingly, the optimization setup presented in Section IV is modified to take into account the effect of touchdown delay. Specifically, the calculation of touchdown conditions in Equation (13) involves numerically solving the system

dynamics presented in Equation (1) for the touchdown delay period. Note that during this period, the actuator is not working yet, thus $u = 0\,\mathrm{N}$. This numerical process currently uses *ode45* function in MATLAB which slows down the entire optimization process by nearly $50\,\%$, from around $2\,\mathrm{s}$ to around $3\,\mathrm{s}$, and can be improved in the future by using an approximated analytical solution.

Experimental verification examined gaits with 4 apex horizontal velocities ($2.5\,\mathrm{m/s}$, $3.0\,\mathrm{m/s}$, $3.5\,\mathrm{m/s}$ and $4.0\,\mathrm{m/s}$) and 3 apex heights ($0.18\,\mathrm{m}$, $0.20\,\mathrm{m}$ and $0.22\,\mathrm{m}$), 12 combinations in total. With reasonable touchdown angles limited by ground friction (slipping occurs below $70°$), the new optimization setup with touchdown delay mechanism was able to find optimal force profiles for 9 out of the 12 combinations. The optimal force profile for the gait featuring $\dot{x}^{apex} = 4.0\,\mathrm{m/s}$, $z^{apex} = 0.18\,\mathrm{m}$ and $\psi^{TD} = 77°$ can be found in Figure 6(a). This force profile, compared to the one shown in Figure 5, does not have the first stage negative force input to reduce the vertical ground reaction force. This is due to the fact that the touchdown delay mechanism closes the time window for that portion. The new force profiles starts directly from the second transition stage. The apex states of this gait in experiments are plotted for each step in Figures 6(b). It can be seen that the system performance at steady state is very close to the expected values, with errors within $\pm 10\,\%$. This gait enabled the single-legged hopper to achieve the maximum forward speed thus far, approximately $3.8\,\mathrm{m/s}$.

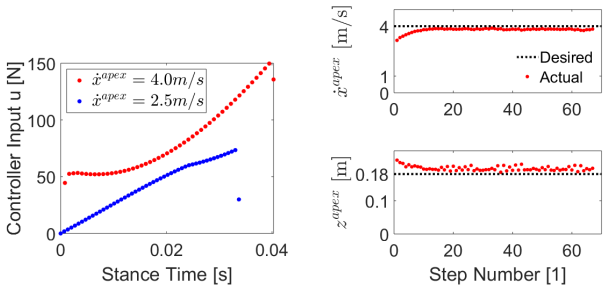

(a) (b)

Fig. 6. Information about the gait featuring $\dot{x}^{apex} = 4.0\,\mathrm{m/s}$, $z^{apex} = 0.18\,\mathrm{m}$ and $\psi^{TD} = 77°$. (a) Optimal force profile. As a comparison, the optimal force profile for gait featuring $\dot{x}^{apex} = 2.5\,\mathrm{m/s}$, $z^{apex} = 0.18\,\mathrm{m}$ and $\psi^{TD} = 78°$ is also plotted. The optimization took into account the touchdown delay mechanism. (b) Achieved apex states per each step from experiments.

The performance of the other 8 gaits can be found in Figure 7, where the colored circles indicate the desired gaits and the colored error bars indicate the actual performance of the gaits. The length of the error bars are dictated by the actual fluctuation of experimental performance, with boundary values being the minimum or maximum steady-state experimental values. For all the 9 tested gaits shown in Figure 7, the actual apex heights are consistently higher than the desired apex heights. This may be due to the drift of reference point. More significantly, the change of desired apex height positively relates to the change of actual apex height. On the other hand, the apex horizontal velocities of the three $2.5\,\mathrm{m/s}$ gaits have greater errors than the other gaits, possibly because of their poorer stability (larger eigenvalues as shown in Figure 4). The other six gaits' apex horizontal velocities are within $\pm 10\,\%$ of their desired values.

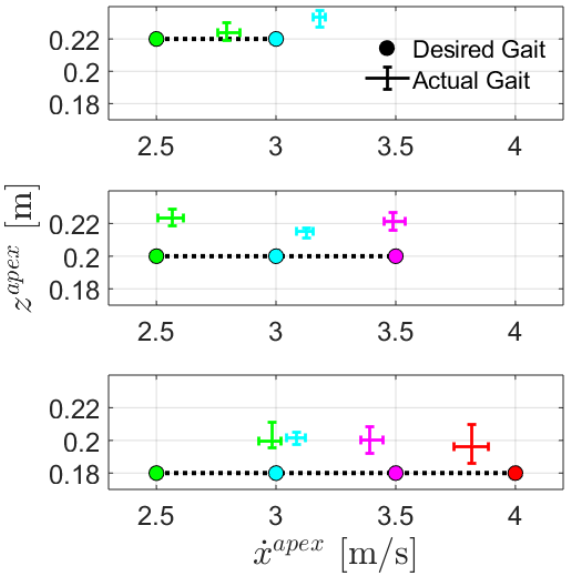

Fig. 7. Achieved steady-state apex states for all the 9 tested gaits.

Overall, the successful implementation on the physical platform and the fast execution speed indicate that it is promising for real-time application. In the future, with improvement on data transmission and gait transition, real-time gait switching can be expected on the physical platform.

VI. CONCLUSIONS

This paper unifies time-based stiffness and rest length modulation as a spring modulation controller for SLIP-like runners. It takes advantage of direct collocation method to handle system dynamics and can generate optimal force input for desired gaits within seconds, which is critical to adaptive legged locomotion. Besides, the shape of the obtained optimal force profiles can potentially inspire new leg controllers on platforms where online optimization is not feasible. The model-based optimization results are verified on hardware, enabling the single-legged hopper to run as fast as $3.8\,\mathrm{m/s}$.

ACKNOWLEDGMENT

The authors gratefully acknowledge the support by the collaborative participation in the Robotics Consortium sponsored by the U.S. Army Research Laboratory under the Collaborative Technology Alliance Program, Cooperative Agreement DAAD 19-01-20012.

REFERENCES

[1] R. J. Full and D. E. Koditschek, "Templates and anchors: neuromechanical hypotheses of legged locomotion on land," *Journal of experimental biology*, vol. 202, no. 23, pp. 3325–3332, 1999.

[2] R. M. Alexander, *Principles of animal locomotion*. Princeton University Press, 2003.

[3] M. H. Raibert, *Legged robots that balance*. MIT press, 1986.

[4] R. Cham and M. S. Redfern, "Changes in gait when anticipating slippery floors," *Gait & posture*, vol. 15, no. 2, pp. 159–171, 2002.

[5] R. Altendorfer, N. Moore, H. Komsuoglu, M. Buehler, H. Brown, D. McMordie, U. Saranli, R. Full, and D. E. Koditschek, "Rhex: A biologically inspired hexapod runner," *Autonomous Robots*, vol. 11, no. 3, pp. 207–213, 2001.

[6] B. Andrews, B. Miller, J. Schmitt, and J. E. Clark, "Running over unknown rough terrain with a one-legged planar robot," *Bioinspiration & biomimetics*, vol. 6, no. 2, p. 026009, 2011.

[7] S. Riese and A. Seyfarth, "Stance leg control: variation of leg parameters supports stable hopping," *Bioinspiration & biomimetics*, vol. 7, no. 1, p. 016006, 2011.

[8] P. Birkmeyer, K. Peterson, and R. S. Fearing, "Dash: A dynamic 16g hexapedal robot," in *2009 IEEE/RSJ International Conference on Intelligent Robots and Systems*. IEEE, 2009, pp. 2683–2689.

[9] A. T. Baisch, C. Heimlich, M. Karpelson, and R. J. Wood, "Hamr3: An autonomous 1.7 g ambulatory robot," in *2011 IEEE/RSJ International Conference on Intelligent Robots and Systems*. IEEE, 2011, pp. 5073–5079.

[10] R. S. Pierre, W. Gosrich, and S. Bergbreiter, "A 3d-printed 1 mg legged microrobot running at 15 body lengths per second," 2018.

[11] K. D. Mombaur, R. W. Longman, H. G. Bock, and J. P. Schlöder, "Open-loop stable running," *Robotica*, vol. 23, no. 1, pp. 21–33, 2005.

[12] J. D. Weingarten, G. A. Lopes, M. Buehler, R. E. Groff, and D. E. Koditschek, "Automated gait adaptation for legged robots," in *IEEE International Conference on Robotics and Automation, 2004. Proceedings. ICRA'04. 2004*, vol. 3. IEEE, 2004, pp. 2153–2158.

[13] J. M. Brown, C. P. Carbiener, J. Nicholson, N. Hemenway, J. L. Pusey, and J. E. Clark, "Fore-aft leg specialization controller for a dynamic quadruped," in *2018 IEEE International Conference on Robotics and Automation (ICRA)*. IEEE, 2018, pp. 1–9.

[14] S. Kuindersma, R. Deits, M. Fallon, A. Valenzuela, H. Dai, F. Permenter, T. Koolen, P. Marion, and R. Tedrake, "Optimization-based locomotion planning, estimation, and control design for the atlas humanoid robot," *Autonomous Robots*, vol. 40, no. 3, pp. 429–455, 2016.

[15] J. Di Carlo, P. M. Wensing, B. Katz, G. Bledt, and S. Kim, "Dynamic locomotion in the mit cheetah 3 through convex model-predictive control," in *2018 IEEE/RSJ International Conference on Intelligent Robots and Systems (IROS)*. IEEE, 2018, pp. 1–9.

[16] S. Feng, E. Whitman, X. Xinjilefu, and C. G. Atkeson, "Optimization-based full body control for the darpa robotics challenge," *Journal of Field Robotics*, vol. 32, no. 2, pp. 293–312, 2015.

[17] A. Wächter and L. T. Biegler, "On the implementation of an interior-point filter line-search algorithm for large-scale nonlinear programming," *Mathematical programming*, vol. 106, no. 1, pp. 25–57, 2006.

[18] A. Hereid, S. Kolathaya, and A. D. Ames, "Online optimal gait generation for bipedal walking robots using legendre pseudospectral optimization," in *2016 IEEE 55th Conference on Decision and Control (CDC)*. IEEE, 2016, pp. 6173–6179.

[19] K. Sreenath, H.-W. Park, I. Poulakakis, and J. W. Grizzle, "Embedding active force control within the compliant hybrid zero dynamics to achieve stable, fast running on mabel," *The International Journal of Robotics Research*, vol. 32, no. 3, pp. 324–345, 2013.

[20] W.-L. Ma, S. Kolathaya, E. R. Ambrose, C. M. Hubicki, and A. D. Ames, "Bipedal robotic running with durus-2d: Bridging the gap between theory and experiment," in *Proceedings of the 20th International Conference on Hybrid Systems: Computation and Control*, 2017, pp. 265–274.

[21] D. J. Blackman, J. V. Nicholson, C. Ordonez, B. D. Miller, and J. E. Clark, "Gait development on minitaur, a direct drive quadrupedal robot," in *Unmanned Systems Technology XVIII*, vol. 9837. International Society for Optics and Photonics, 2016, p. 98370I.

[22] A. Seyfarth, H. Geyer, M. Günther, and R. Blickhan, "A movement criterion for running," *Journal of biomechanics*, vol. 35, no. 5, pp. 649–655, 2002.

[23] O. Von Stryk, "Numerical solution of optimal control problems by direct collocation," in *Optimal Control*. Springer, 1993, pp. 129–143.

[24] M. S. Jones, "Optimal control of an underactuated bipedal robot," 2014.

[25] A. Goswami, B. Espiau, and A. Keramane, "Limit cycles and their stability in a passive bipedal gait," in *Robotics and Automation, 1996. Proceedings., 1996 IEEE International Conference on*, vol. 1. IEEE, 1996, pp. 246–251.

[26] R. S. Pierre and S. Bergbreiter, "Gait exploration of sub-2 g robots using magnetic actuation," *IEEE Robotics and Automation Letters*, vol. 2, no. 1, pp. 34–40, 2016.

[27] N. Doshi, K. Jayaram, S. Castellanos, S. Kuindersma, and R. J. Wood, "Effective locomotion at multiple stride frequencies using proprioceptive feedback on a legged microrobot," *Bioinspiration & biomimetics*, 2019.